

Comparison of Different Additively Manufactured Ti6Al4V Scaffold Designs

Sachin Singh*, J.S. Saini, and Rojdeep Singh

Department of Mechanical Engineering, Thapar Institute of Engineering and Technology, Patiala - 147 004, India

*E-mail: sachin.singh@thapar.edu

ABSTRACT

The cellular structures, a repeated array of unit cells in all three directions, are lightweight and resist bending and buckling due to their intricate structural organisation. These structures allow tailoring the mechanical properties of the biomaterial structure near the surrounding bones, which helps reduce the stress shielding effect. Over the years, various fabrication processes have been introduced and evolved to produce cellular (porous) structures with unique mechanical properties, biocompatibility, corrosion rate, degradation rate, etc. In the current work, CAD models of titanium scaffolds have been designed and manufactured by 3D printing for improved performance within the body. In the present work, scaffolds with mechanical properties equivalent to that of the trabecular bone in the human body were developed. Three types of scaffolds were designed with porosity in the range of 84 % – 90 %. Experimental investigations showed that Young's modulus and compression strength of the scaffolds were in the ranges of 0.32 - 1.15 GPa and 10 - 50 MPa, respectively, which correlated with the trabecular bone's mechanical properties. Numerical modeling is performed to predict Young's modulus, stress distribution, and failure under compressive loading of designed scaffolds with different unit cell geometry.

Keywords: Additive manufacturing; Ti6Al4V; Scaffold; Biomedical, Finite element

1. INTRODUCTION

Titanium and its alloys are commonly used for medical implants due to their excellent mechanical properties, good resistance to corrosion, biocompatibility, and high strength-to-weight ratio¹. The elastic modulus of titanium alloy is around 110 GPa. However, it lies in the ranges of 4 – 30 GPa for cortical bone and 0.2 – 2 for trabecular bone, depending on the bone anatomy in the human body²⁻³. High Young's modulus of titanium causes the stress shielding effect due to the relative difference in stiffness of the titanium implant and the adjoining bone, which affects the implant's life. Therefore, lighter implants with mechanical properties closer to that of the replaced bone must be built. This necessitates the implants to be made as porous structures. The porosity in the structure can be given by using cellular lattice structures. Nowadays, the fabrication of metal components using Additive Manufacturing (AM) is a promising technology. Selective Laser Melting (SLM), one of the AM techniques, can be used to build complex 3D components such as cellular lattice structures⁴⁻⁵.

Researchers have done considerable work on different lattice structures to vary the porosities and strength of the structures fabricated using the SLM process. The shape of unit cells influences the mechanical performance of the porous implant⁶. Li¹, *et al.* found that the electron beam melting produced titanium (Ti6Al4V) scaffolds with different porosities, which had a yield strength between 89.7 and 328.1 MPa, a compressive strength between 110.4 MPa and 366.5 MPa, and Young's modulus between 2.72 and 64.76 GPa. The

sample with a porosity of around 51 % had Young's modulus as that of cortical bone. Parthasarathy², *et al.* fabricated the structures with porosity ranging from 49.75 % to 70.32 % using pore and strut size variations. It was found that the structures with porosities between 50 % - 70 % satisfied the mechanical properties required for craniofacial applications. Yan⁷, *et al.* fabricated the gyroid cellular lattice structures with a unit cell varying from 2 - 8 mm. Young's modulus and yield strength were found to increase with the decrease in the unit cell size. Authors⁸⁻⁹ fabricated different types of lattice topology using SLM. It was found that the unit cell topology, cell size, and relative density were the significant parameters that affect the properties of lattice structures. Han, *et al.*¹⁰ designed porous scaffolds based on Face-Centered Cubic (FCC), Cubic Close-Packed (CCP), Spherical Hollow Cubic (SHC), and Body-Centered Cubic (BCC) topologies. Zhao¹¹, *et al.* studied the effect of unit cell type and pore size on the fatigue properties and cell affinity for SLM fabricated Ti6Al4V scaffolds. It was found that the fatigue properties and the compressive strength of the octahedron scaffolds are higher than those of tetrahedron scaffolds. Zhang¹², *et al.* designed and fabricated a titanium unit cell to mimic trabecular bone structure. The scaffolds' mechanical properties, collapse behavior, and failure mechanism were studied. It was found that the modulus of the scaffold was in the range of 0.39-0.618 GPa, which was near to that of a bone. Wang¹³, *et al.* developed Ti6Al4V scaffolds and successfully carried out in vivo studies to demonstrate their biological performance in terms of bone regeneration and bone-implant fixation. Later, Chen¹⁴, *et al.* showed that 3D printed scaffolds with pore size 500 μm having porosity of 60 % performed best in vitro and in vivo studies.

Some of the researchers have used Finite Element Methods (FEM) to analyze the different lattice structures. Li¹⁵, *et al.* developed a full-scale 3D Finite Element (FE) model to investigate the deformation of lattice structure due to compression loading. The numerical results were validated experimentally. Rotta¹⁶, *et al.* used FE analysis to design scaffolds from different types of primitives, i.e., spheres and cubes. It was found that the size of the pores had more influence on the elastic modulus than the shape of the pores. Deng¹⁷, *et al.* clubbed in vivo experiments with Computational Fluid Dynamics (CFD) to investigate the fluid flow velocity in scaffolds. Sercombe¹⁸, *et al.* created scaffolds based on topology optimization with three nominal solid fractions: 7 %, 10 %, and 15 %. It was found that the first failure in these structures occurred in struts; thereafter, the shear failure occurred at 45°. Weißmann¹⁹, *et al.* investigated cubic, pyramidal, and twisted types of scaffold designs, which were fabricated using the SLM process. The porosities and elastic modulus of the scaffolds varied from 43 %-80 % and 3.4 GPa - 26.3 GPa, respectively. It was found that there was a linear correlation between the strengths and the strut width-to-diameter ratio. Few authors²⁰⁻²¹ proposed scaffolds with graded porosity resembling the structure of human bone to promote bone regeneration. The authors also enhanced bone tissue regeneration by performing various post-processing operations on the 3D-printed Ti6Al4V scaffolds. Huang²², *et al.* applied a coating containing calcium, oxygen, and phosphorous on the scaffolds by hydrothermal treatment followed by microarc oxidation. Developed scaffolds showed enhanced protein adsorption, adhesion, and osseointegration. Zarei²³, *et al.* post-processed the PLA-Ti6Al4V scaffolds by plasma treatment with oxygen and air to increase their hydrophilicity and roughness. Post-processed scaffolds showed better mechanical and bioactivity properties compared to the unprocessed ones.

As per the literature review, a structure's mechanical properties depend on the material's relative density and the geometry or topology of the unit cell. Most published literature concentrates on designing scaffolds with mechanical properties comparable to cortical bone. However, Young's modulus and compressive yield strength for trabecular bone is less than that of cortical bone, and very little literature is available on designing scaffolds with mechanical properties in the range of trabecular bone. To address this shortcoming in the current work, three different scaffold designs, i.e., Face-Centered Cubic (FCC), Twisted With Crossing Struts (TCS), and Body-Centered Cubic With Vertical Struts (BCCz), were designed and 3D printed using Ti6Al4V material. Experimental studies were performed to evaluate Young's modulus and the compressive strength of the fabricated samples. Thereafter, finite element modeling was performed, and the experimental results were validated with the numerical results.

2. METHODOLOGY

The following section shows the design, methods, and steps used in the present work.

2.1 Scaffold Design

Three scaffold designs were selected from the literature

that showed the minimum elastic modulus in the range of 5 - 25 GPa^{19,24}. These designs were modified in terms of cell size and structure to reduce the elastic modulus further and make it comparable with that of trabecular bone. Scaffolds were designed using PTC Creo Parametric 6.0.2.0 software. According to ASTM standards, the cubic lattice was designed with 13.4 mm width and 26.4 mm height. A single unit cell of 3 mm with 0.4 mm strut thickness was first generated and repeated in three dimensions. The models were exported from the modeling software into the Magic software using the STL format to prepare the file for the metal 3D printer. The CAD models of the different designs are given in Fig. 1.

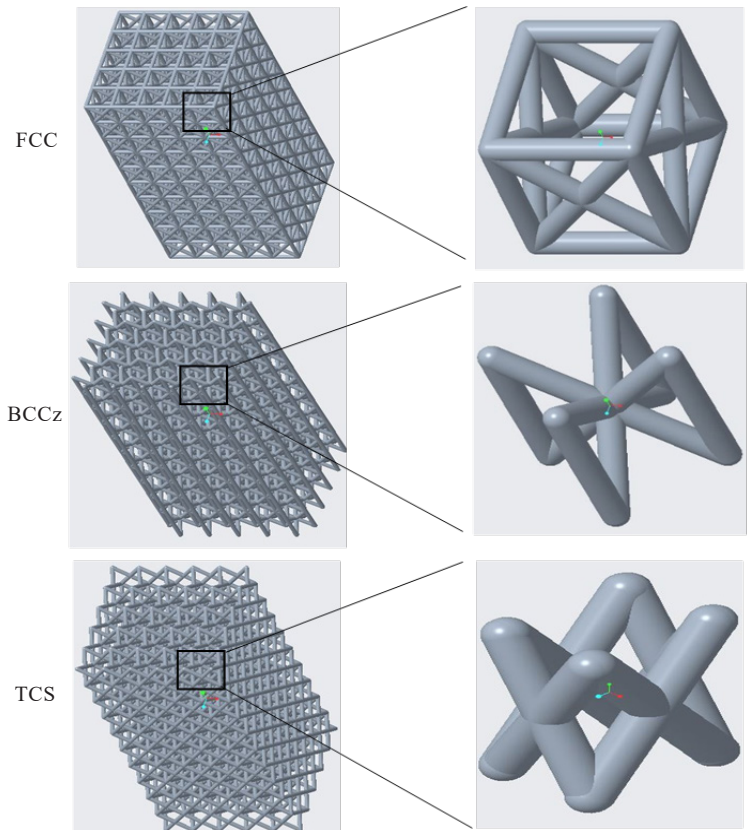


Figure 1. CAD Models of lattice structures with their corresponding unit cells.

2.2 Selective Laser Melting

The specimens were made as per ASTM E9 using Ti6Al4V powder with a particle size of around 4-40 μm in an argon atmosphere (Fig. 2(a)). These designs were 3D printed using a selective laser melting machine (make: EOSIMT 280) (Fig. 2(b)). Lattice structures were 3D printed with a laser power of 340 W, layer thickness of 60 μm , hatch distance of 0.12 mm, and scanning speed of 1250 mm/sec. Heat treatment was performed on the fabricated structures at 800 $^{\circ}\text{C}$ for 90 min. The surface roughness of the 3D printed scaffolds was in the range of 10 - 12 μm .

2.3 Mechanical Testing

The mechanical testing of the specimens was done through uniaxial compression tests using a compression (model: TJ146) machine (Fig. 3(a)). The testing was carried

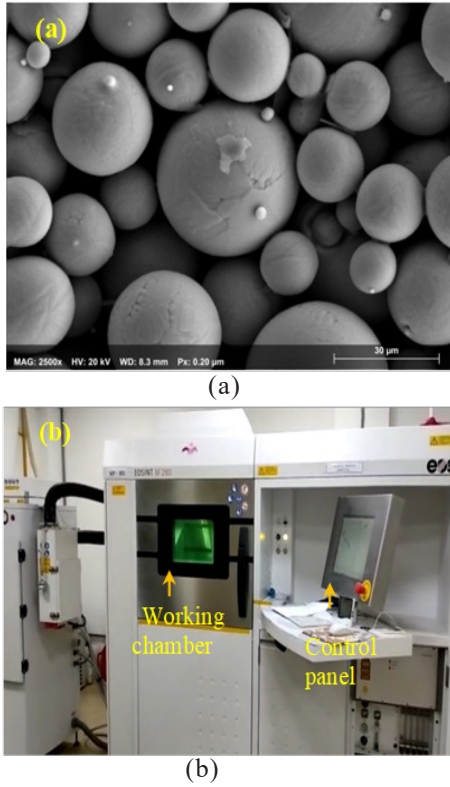


Figure 2. (a) SEM image of the Ti6Al4V powder, and (b) Selective laser melting machine.

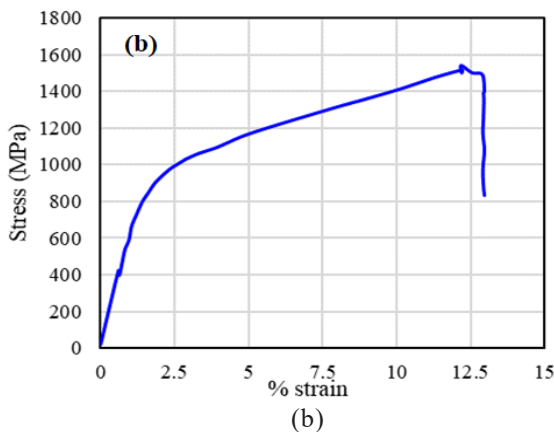
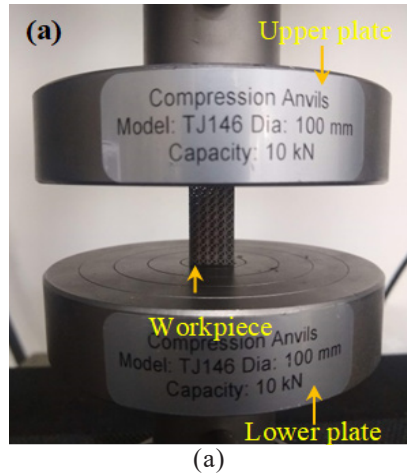


Figure 3. (a) Test set up for uniaxial compression testing, and (b) Compression stress-strain curve for a fully dense Ti64 component.

out using a cross-head speed of 2 mm/min. at room temperature on five different specimens of each design. Scanning electron microscopy (SEM) images were taken using JSM 6200 (JEOL, Japan) equipment to study the surface of lattice structures.

2.4 Porosity

The porosity of the fabricated lattice structures was measured to verify the accuracy of the fabricated process with the CAD designs. For scaffolds, the numerical porosity of the CAD models, V_n was evaluated using Eqn. (1).

$$V_n = \left(1 - \frac{v_{sc}}{v_{cu}}\right) \times 100 \% \quad (1)$$

where, v_{sc} is the volume of the porous scaffold, and v_{cu} is the overall volume of a solid structure with the exact outer dimensions. The porosities of the CAD models were then compared with the experimental porosity of SLM-manufactured scaffolds, V_e which was calculated using Eqn. (2).

$$V_e = \left(1 - \frac{v_{wd}}{v_{total}}\right) \times 100 \% \quad (2)$$

where, v_{wd} is the volume of water displaced and v_{total} is the volume of a solid scaffold²⁵.

2.5 Finite Element Analysis

3D scaffold models developed by the Creo Parametric were imported (STEP files) in Abaqus software to find the compressive strength. The engineering stress-strain properties of the fully dense component (Fig. 3(b)) were extracted and changed into the true stress-strain properties using Eqn. (3-4). These were used as input in elastoplastic material used for numerical model.

$$\sigma_t = \sigma_e \times (1 + \varepsilon_e) \quad (3)$$

$$\varepsilon_t = \ln(1 + \varepsilon_e) \quad (4)$$

where, σ_t , σ_e are true and engineering stress and ε_e , ε_t are engineering and true strain, respectively.

For the boundary conditions, one of the surfaces was subjected to a displacement of 2 mm, while the other was fixed in rotation and translation. Tetrahedral elements were used to mesh the 3D model to accurately capture the unit cell geometry and post-processing results.

3. RESULTS AND DISCUSSION

The following section shows the results for the three scaffold designs used in the present work.

3.1 Porosity

For safe vascularization, good cell migration, and sufficient surface area for cell adherence, porosity must be greater than 50 %. The porosity of scaffolds was determined both numerically and experimentally. As shown in Table 1, the numerical porosity obtained was higher than the experimental values. This can be explained by the fact that CAD models assume that the surfaces are perfectly smooth and have no surface roughness, whereas in 3D printed scaffolds, various uncontrollable parameters in the SLM process cause surface abnormalities, especially high surface roughness. Figure 4 shows the highly rough surface of the 3D printed samples,

and also shows that the strut thickness in all three samples was greater than the designed strut thickness, i.e., 0.4 mm. As a result, the porosity of the scaffolds decreases.

Table 1. Porosity for the different scaffolds

Samples	Numerical porosity (%)	Experimental porosity (%)
FCC	84.68	74.68
BCCz	88.39	78.00
TCS	89.86	78.90

3.2 Mechanical Properties

Figure 5(a) displays the compression stress-strain curves of the manufactured scaffolds. Every stress-strain curve exhibited typical metal foam behavior. It can be seen that the stress grew linearly upto a certain point. Its slope dropped beyond this point, or after the proportionality limit. The strut begins to bend at this point. A subsequent rise in load causes the strut to break. The struts in all the designs fail along the 45° plane. The failure of the scaffolds during the compression testing was also simulated numerically using finite element

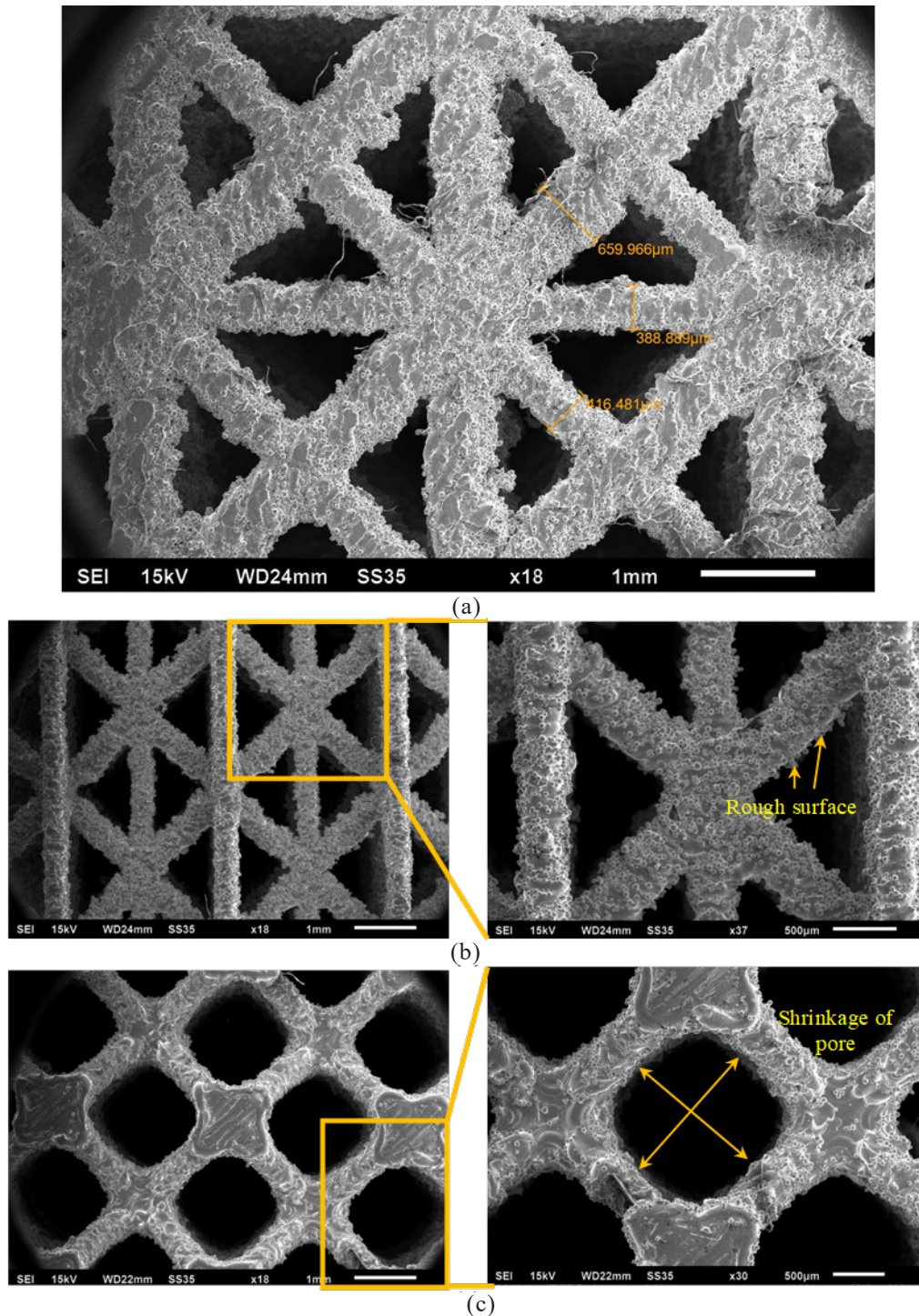


Figure 4. Scanning electron image showing strut surface features of various 3D printed scaffolds (a) FCC (b) BCCz (c) TCS.

analysis. Figure 6(a)–(c) compares compression processes between experimental and numerical results.

Simulated results showed that the magnitude of Von Mises (VM) stress generated is highest in FCC, followed by BCCz and TCS scaffolds. FCC structure has more straight struts (vertical and horizontal), which offer direct resistance to deformation that increases its Young's modulus (stiffness) and stress-carrying capacity, resulting in high VM stress²⁶. BCCz scaffold's unit cell contains only vertical struts; therefore, stiffness is reduced, and so are the VM stresses. While the TCS structure has all inclined struts. As a result, it had the least Young's modulus. In addition, simulated results showed fracture initiation points of the struts for different scaffolds. As shown in Fig. 6(a), high VM stress concentration on the struts junction in the FCC structure initiates the struts failure which propagated along the 45° plane. The bending of struts in BCCz and TCS structures leads to scaffold failure. Compared to FCC scaffolds, stress concentration is less dominant in BCCz and TCS scaffolds, which have a more uniform stress distribution. Thus, BCCz and TCS have excellent stress carrying capacity and can be preferred over FCC scaffolds.

Figure 5(b) compares the experimental and numerical values of Young's modulus for various scaffolds. However, the error in the simulated results was around 50 %. Error greater than 50 % is also reported in published literature²⁷. The primary cause of the error is micro-level porosities in actual 3D printed struts of the scaffolds. These micro-level porosities are the crack initiation point, as revealed by SEM analysis shown in Fig. 7. As a result, scaffold failure starts even for low values of stresses, but such impurities are not considered during the present simulation. In addition, the 3D printed material properties are anisotropic, but during the simulation, studies are performed by assuming it as an isotropic material.

Young's modulus for the cortical bone range lies within 4 - 30 GPa, and the trabecular bone range is 0.2 - 2 GPa. Yield strength reported in the literature for cortical and trabecular bone are 20 -193 MPa and 2 - 80 MPa, respectively³. Table

2 compares the 3D printed scaffolds in the current work with those in the published literature with a similar porosity, i.e., greater than 60 %. It is found that the elastic modulus and yield strength of the as-built scaffolds in this study are in good agreement with the mechanical properties of the trabecular bone, reducing the chances of stress shielding and making them suitable for biomedical applications.

4. CONCLUSIONS

The current work examined the stiffness and strength characteristics of three different designs of scaffolds manufactured using the SLM process. The major findings of the work are as follows:

- Three different designs of scaffolds, viz., FCC, BCCz, and TCS, were successfully 3D printed using the SLM process.
- All the designs have a porosity greater than 70 %, which is helpful for cell and bone generation.
- The designed scaffolds' elastic modulus and yield strength lie between 0.5-1.14 GPa and 20 – 43 MPa, respectively. The properties are in good agreement with human bones.
- Numerical results accurately predict the failure mode for various scaffolds based on their cell geometry. However, the discrepancy between the magnitude of Young's modulus is primarily due to several experimental factors that are not considered during the present numerical model.

In the current work, prime emphasis was given to designing and developing the scaffold with mechanical properties in the range of the trabecular bone. However, biocompatibility regarding cell seeding and bone growth is also essential for scaffolds. The scaffold's shape and size also influence these properties.

In future work, such investigations (in vitro /in vivo) can be performed to confirm the biocompatibility of the scaffolds. In addition, more realistic numerical models can be developed

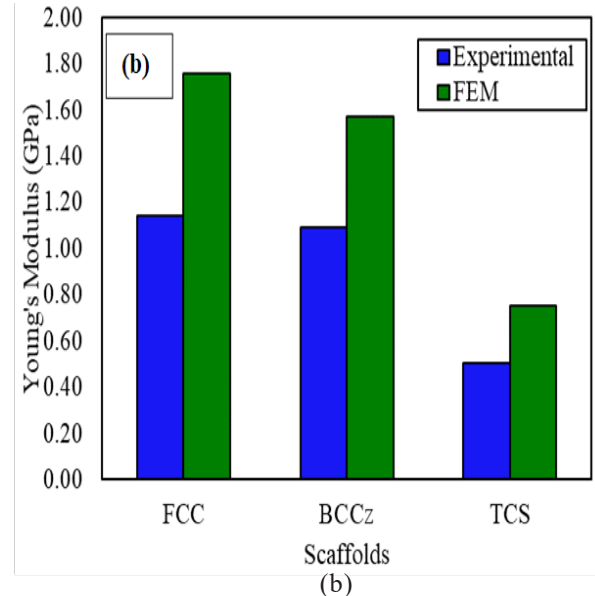
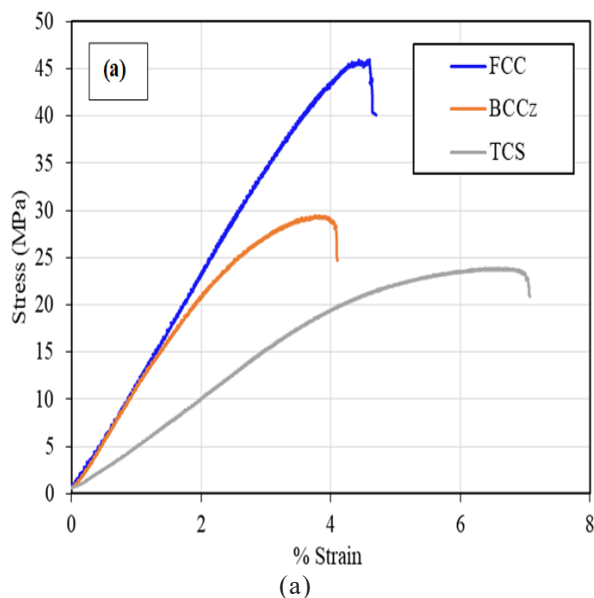


Figure 5. (a) Experimental stress-strain relationship for each scaffold during compression testing, and (b) Experimental and numerical values of Young's modulus.

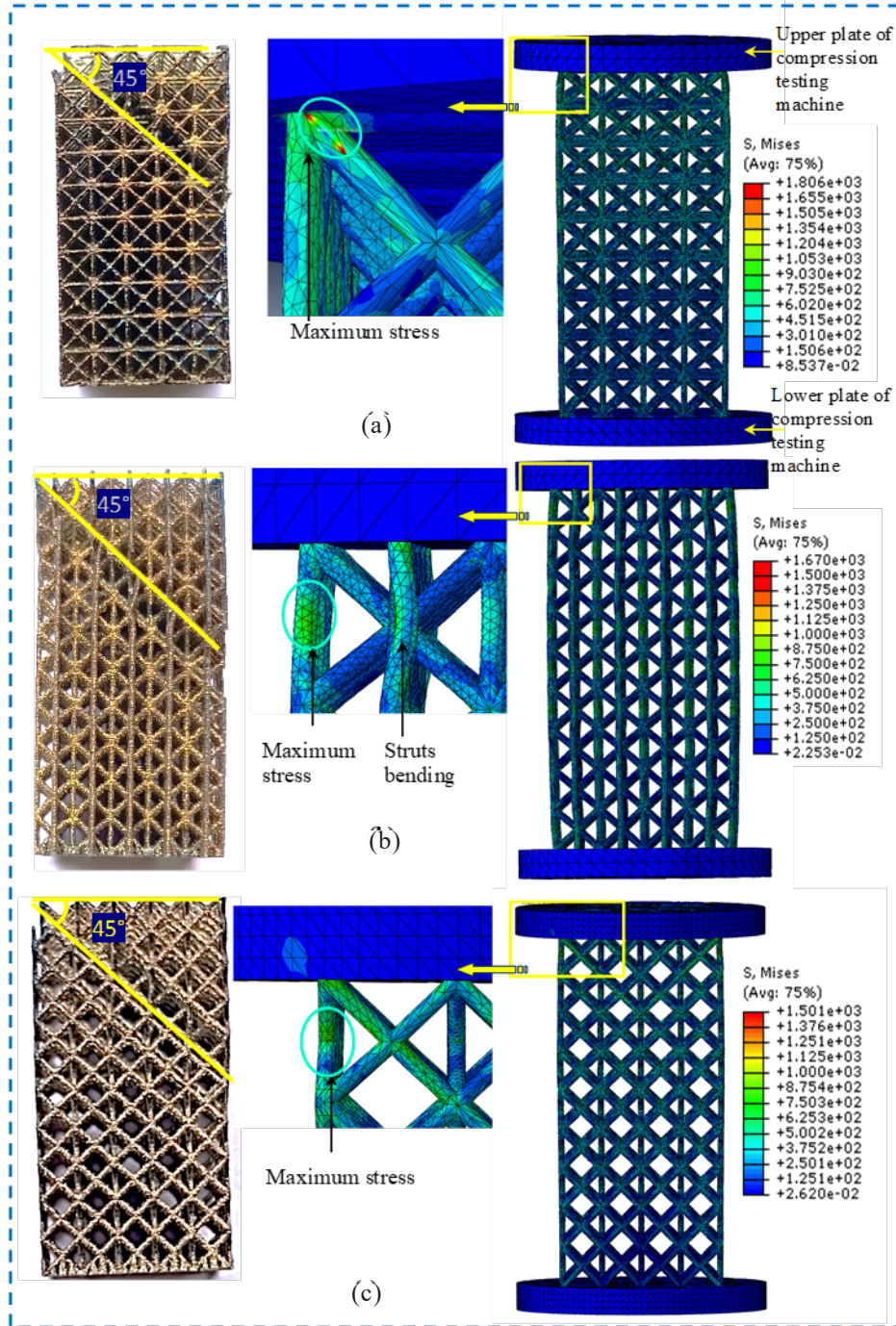


Figure 6. Failure of the scaffolds during the compression testing (a) FCC, (b) BCCz, and (c) TCS.

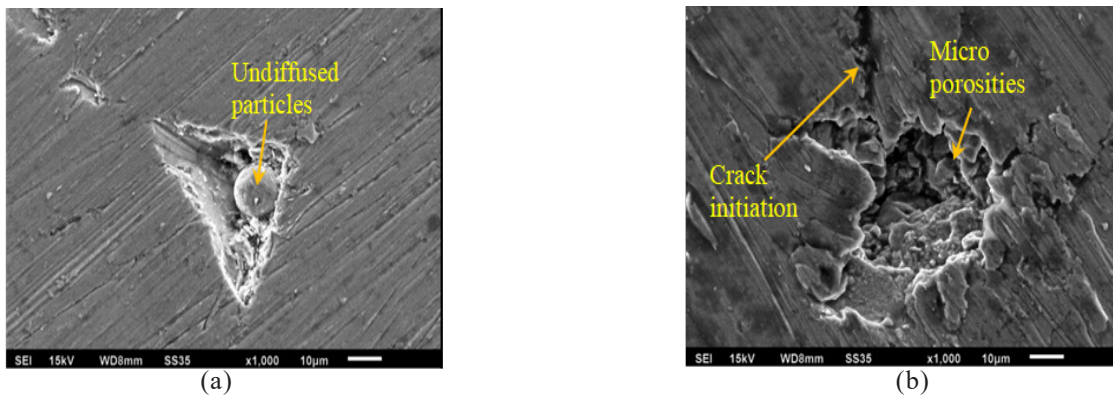


Figure 7. Location of the crack's initiation inside the strut under compression loading.

Table 2. Mechanical properties of different porous scaffolds in this study in comparison with results from previous literature

Pore structure	Young's modulus (GPa)	Compressive yield Stress (MPa)	Reference
FCC	1.14	42.80	Present study
BCCz	1.09	23.60	Present study
TCS	0.503	20.10	Present study
Gyroid	10.60	22.44	[3]
Triplic periodic minimal surface	2.40	233	[20]
Graded FCC	6.10	185	[21]
BCC	4.7	153	[28]
Twisted design	3.40	103.70	[29]
Trabecular bone	0.2 - 2	2 - 80	[3]

to predict mechanical properties in a more accurate manner which can optimize the geometry.

ACKNOWLEDGEMENT

This work was financially supported (DSF contract ID:2023-9445) by the Dassault Systèmes Foundation, Pune, Maharashtra (India) and Thapar Institute of Engineering and Technology, Patiala, Punjab (India).

REFERENCES

- Li, X.; Wang, C.; Zhang, W. & Li, Y. Fabrication and compressive properties of Ti6Al4V implant with honeycomb-like structure for biomedical applications. *Rapid Prototyp. J.*, 2010, **16**(1), 44–49. doi: 10.1108/13552541011011703.
- Parthasarathy, J.; Starly, B.; Raman, S. & Christensen, A. Mechanical evaluation of porous titanium (Ti6Al4V) structures with electron beam melting (EBM). *J. Mech. Behav. Biomed. Mater.*, 2010, **3**(3), 249–259. doi: 10.1016/j.jmbbm.2009.10.006.
- Zaharin, H.A.; Rani, A.M.A.; Azam, F.I.; Ginta, T.L.; Sallih, N.; Ahmad, A.; Yunus, N.A.; & Zulkifli, T.Z.A. Effect of unit cell type and pore size on porosity and mechanical behavior of additively manufactured Ti6Al4V scaffolds. *Materials (Basel)*, 2018, **11**(12), 2402 (1-15). doi: 10.3390/ma11122402.
- Santorinaios, M.; Brooks, W.; Sutcliffe, C.J. & Mines, R. A.W. Crush behaviour of open cellular lattice structures manufactured using selective laser melting. *WIT Trans. Built Environ.*, 2006, **85**, 481–490. doi: 10.2495/HPSM06047.
- Koju, N.; Niraula, S. & Fotovvati, B. Additively Manufactured porous Ti6Al4V for bone implants: *A Review. Metals*, 2022, **12**(4), 687 (1-34). doi: 10.3390/met12040687.
- Li, J.; Chen, D.; Luan, H.; Yan, W. & Fan, Y. Mechanical performance of porous implant with different unit cells. *J. Mech. Med. Biol.*, 2017, **17**(6), 1–18. doi: 10.1142/S0219519417501019.
- Yan, C.; Hao, L.; Hussein, A. & Raymont, D. Evaluations of cellular lattice structures manufactured using selective laser melting. *Int. J. Mach. Tools Manuf.*, 2012, **62**, 32–38. doi: 10.1016/j.ijmachtools.2012.06.002.
- Gumruk, R.; Mines, R.A.W. & Karadeniz, S. Static mechanical behaviours of stainless steel micro-lattice structures under different loading conditions. *Mater. Sci. Eng. A*, 2013, **586**, 392–406. doi: 10.1016/j.msea.2013.07.070.
- Lipowiecki, M. & Brabazon, D. Design of bone scaffolds structures for rapid prototyping with increased strength and osteoconductivity. *Adv. Mater. Res.*, 2010, **83–86**, 914–922. doi: 10.4028/www.scientific.net/AMR.83-86.914.
- Han, C.; Yan, C.; Wen, W.; Xu, T.; Li, S.; Liu, J.; Wei, Q. & Shi, Y. Effects of the unit cell topology on the compression properties of porous Co-Cr scaffolds fabricated via selective laser melting. *Rapid Prototyp. J.*, 2017, **23**(1), 16–27. doi: 10.1108/RPJ-08-2015-0114.
- Zhao, D. Huang, Y.; Ao, Y.; Han, C.; Wang, Q.; Li, Y.; Liu, J.; Wei, Q. & Zhang, Z. Effect of pore geometry on the fatigue properties and cell affinity of porous titanium scaffolds fabricated by selective laser melting. *J. Mech. Behav. Biomed. Mater.*, 2018, **88**, 478–487. doi: 10.1016/j.jmbbm.2018.08.048.
- Zhang, L.; Liu, L.; Lv, L.; Gao, L.; Liu, N.; Wang, X. & Ye, J. Mechanical behavior of a titanium alloy scaffold mimicking trabecular structure. *J. Orthop. Surg. Res.*, 2020, **15**(1), 1–11. doi: 10.1186/s13018-019-1489-y.
- Wang, H.; Su, K.; Su, L.; Liang, P.; Ji, P. & Wang, C. Comparison of 3D-printed porous tantalum and titanium scaffolds on osteointegration and osteogenesis. *Mater. Sci. Eng. C*, 2019, **104**, 109908. doi: 10.1016/j.msec.2019.109908.
- Chen, Z.; Yan, X.; Yin, S.; Liu, L.; Liu, X.; Zhao, G.; Ma, W.; Qi, W.; Ren, Z.; Liao, H.; Liu, M.; Cai, D. & Fang, H. Influence of the pore size and porosity of selective laser melted Ti6Al4V ELI porous scaffold on cell proliferation, osteogenesis and bone ingrowth. *Mater. Sci. Eng. C*, 2020, **106**, 110289. doi: 10.1016/j.msec.2019.110289.
- Li, P.; Wang, Z.; Petrinic, N. & Siviour, C. R. Deformation behaviour of stainless steel microlattice structures by selective laser melting. *Mater. Sci. Eng. A*, 2014, **614**, 116–121. doi: 10.1016/j.msea.2014.07.015.
- Rotta, G.; Seramak, T. & Zasińska, K. Estimation of Young's Modulus of the Porous Titanium Alloy with the

- Use of Fem Package. *Adv. Mater. Sci.*, 2015, **15**(4), 29–37.
doi: 10.1515/adms-2015-0020.
17. Deng, F.; Liu, L.; Li, Z. & Liu, J. 3D printed Ti6Al4V bone scaffolds with different pore structure effects on bone ingrowth. *J. Biol. Eng.*, 2021, **15**(1), 1–13.
doi: 10.1186/s13036-021-00255-8.
 18. Sercombe, T.B.; Xu, X.; Challis, V.J.; Green, R.; Yue, S.; Zhang, Z. & Lee, P.D. Failure modes in high strength and stiffness to weight scaffolds produced by Selective Laser Melting. *Mater. Des.*, 2015, **67**, 501–508.
doi: 10.1016/j.matdes.2014.10.063.
 19. Weißmann, V.; Wieding, J.; Hansmann, H.; Laufer, N.; Wolf, A. & Bader, R. Specific yielding of selective laser-melted Ti6Al4V open-porous scaffolds as a function of unit cell design and dimensions. *Metals*, 2016, **6**(7), 166 (1-19) .
doi: 10.3390/met6070166.
 20. Liao, B.; Xia, R.F.; Li, W.; Lu, D. & Jin, Z. M. 3D-Printed Ti6Al4V scaffolds with graded triply periodic minimal surface structure for bone tissue engineering. *J. Mater. Eng. Perform.*, 2021, **30**(7), 4993–5004.
doi: 10.1007/s11665-021-05580-z.
 21. Yu, A.; Xu, W.; Lu, X.; Tamaddon, M.; Liu, B.; Tian, S.; Zhang, C.; Mughal, M.A. Zhang, J.; & Liu, C. Development and characterizations of graded porous titanium scaffolds via selective laser melting for orthopedics applications. *Trans. Nonferrous Met. Soc. China*. 2023, **33**(6), 1755–1767.
doi: 10.1016/S1003-6326(23)66219-3.
 22. Huang, L.; Cai, B.; Huang, Y.; Wang, J.; Zhu, C.; Shi, K., & Zhang, L. Comparative study on 3D printed Ti6Al4V scaffolds with surface modifications using hydrothermal treatment and microarc oxidation to enhance osteogenic activity. *Acs Omega*, 2021, **6**(2), 1465-1476.
doi: 10.1021/acsomega.0c05191.
 23. Zarei, M.; Dargah, M.Z.; Azar, M.H.; Alizadeh, R.; Mahdavi, F.S.; Sayedain, S.S.; Kaviani, A.; Asadollahi, M.; Azami, M. & Beheshtizadeh, N. Enhanced bone tissue regeneration using a 3D-printed poly(lactic acid)/Ti6Al4V composite scaffold with plasma treatment modification. *Sci. Rep.*, 2023, **13**(1), 3139 (1–18).
doi: 10.1038/s41598-023-30300-z.
 24. Sallica-Leva, E.; Jardini, A.L. & Fogagnolo, J.B. Microstructure and mechanical behavior of porous Ti–6Al–4V parts obtained by selective laser melting. *J. Mech. Behavior of Biomed. Mater.*, 2013, **26**, 98-108.
doi: 10.1016/j.jmbbm.2013.05.011.
 25. Soro, N.; Attar, H.; Wu, X. & Dargusch, M.S. Investigation of the structure and mechanical properties of additively manufactured Ti-6Al-4V biomedical scaffolds designed with a Schwartz primitive unit-cell. *Mater. Sci. Eng. A*, 2019, **745**, 195–202.
doi: 10.1016/j.msea.2018.12.104.
 26. Smith, M.; Guan, Z. W.; & Cantwell, W. J. Finite element modelling of the compressive response of lattice structures manufactured using the selective laser melting technique. *Int. J. Mech. Sci.*, 2013, **67**, 28-41.
doi: 10.1016/j.ijmecsci.2012.12.004.
 27. Hazlehurst, K.; Wang, C.J.; & Stanford, M. Evaluation of the stiffness characteristics of square pore CoCrMo cellular structures manufactured using laser melting technology for potential orthopaedic applications, *Materials & Design*, 2013, **51**, 949-955.
doi: 10.1016/j.matdes.2013.05.009.
 28. Yu, G.; Li, Z.; Li, S.; Zhang, Q.; Hua, Y.; Liu, H. & Wang, X. The select of internal architecture for porous Ti alloy scaffold: A compromise between mechanical properties and permeability, *Materials & Design*, 2020, **192**, 108754.
doi: 10.1016/j.matdes.2020.108754.
 29. Weißmann, V.; Bader, R.; Hansmann, H.; & Laufer, N. Influence of the structural orientation on the mechanical properties of selective laser melted Ti6Al4V open-porous scaffolds, *Materials & Design*, 2016, **95**, 188-197.
doi: 10.1016/j.matdes.2016.01.095.

CONTRIBUTORS

Dr Sachin Singh is working as an Assistant Professor in the Mechanical Engineering Department at Thapar Institute of Engineering and Technology, Patiala, Punjab. His areas of interest include: 3D printing.

In the current study, he was involved in the finite element modeling, result analysis, and writing of the current manuscript.

Dr J.S. Saini is working as a Professor in the Mechanical Engineering Department at Thapar Institute of Engineering and Technology, Patiala, Punjab. His areas of specialisation are design and analysis, polymer composites and the 3D printing process.

In the current study, he was involved in the literature review, material selection, and analysis of the results.

Mr Rojdeep Singh was an ME student in the Mechanical Engineering Department at Thapar Institute of Engineering and Technology, Patiala, Punjab.

In the current study, he was involved in experimental testing and analysis of scaffolds.